

An SSPM-Based High-Speed Near-Infrared Photometer for Astronomy

S.S. Eikenberry, G.G. Fazio, S.M. Ransom

Harvard-Smithsonian Center for Astrophysics

60 Garden St., Cambridge, MA 02138

Received _____; accepted _____

arXiv:astro-ph/9607107v1 22 Jul 1996

ABSTRACT

We describe the design, operation, and performance of a new high-speed infrared photometer using the Solid-State Photomultiplier (SSPM) detector. The SSPM was developed by Rockwell International Science Center and has single-photon counting capability over the 0.4-28 micron wavelength range, intrinsic time response of order 1 ns, and low detector noise (Petroff, *et al.*, 1987). We have operated a 200x200-micron back-illuminated SSPM in a liquid-helium cooled dewar with a room-temperature transimpedance amplifier output. Single photon pulses can be easily distinguished above the amplifier noise. The individual photon pulses are binned at a selectable time resolution ranging from $5\mu\text{s}$ to 64 ms, and then written to Exabyte tape. In the first astronomical application of such a device, we have made observations of the Crab Nebula pulsar and Her X-1 at near-infrared wavelengths (J-, H-, and K-bands), and we present the instrument sensitivities established by these observations. We discuss other astronomical observations which are either planned or currently underway. Finally, we present design specifications and predicted performances for a second-generation SSPM high-speed infrared photometer.

1. Introduction

The field of high-speed infrared photometry is one that has existed for many years, but has until now developed very slowly. The range of work done with high-speed near-IR photometers is wide and varied, from observations of pulsars (both rotation- and accretion-powered), X-ray binaries, and cataclysmic variables to applications in IR interferometry, planetary occultations, and lunar occultations. However, the amount of work has been limited, largely due to the relatively poor performance of typical near-IR detectors (e.g. InSb and HgCdTe - see Lundgren (1994); Pipher *et al.*, (1995); Hodapp *et al.*, (1995)) at high speed operation (sampling rates greater than ~ 100 Hz). The appearance of a new technology, that of the Solid-State Photomultiplier, promises to change this state of affairs.

The Solid-State Photomultiplier (SSPM), developed by Rockwell International Science Center (RISC), is a Si:As detector with single-photon counting capability over the wavelength range from $0.4 - 28 \mu\text{m}$, intrinsic time response of order 1 ns, and low detector noise. As such, it provides great advantages over previous high-speed IR detectors in terms of both sensitivity and time resolution. For instance, our first-generation photometer provides 1000 times the time resolution and 2.6 times the signal-to-noise (at 1 kHz) of the Caltech InSb-based high-speed photometer (Lundgren, 1994). Thus, the SSPM for the first time brings high-speed IR photometry into the realm of competition with high-speed optical photometry, which relies on the well-developed technology of photomultiplier tubes (PMTs).

2. Detector

The basic operating principle of the SSPM is that of a blocked-impurity band (BIB) detector operated in avalanche mode. As shown in Figure 1(a), a layer of arsenic-doped silicon is deposited on the silicon substrate, with a blocking layer of undoped Si between the Si:As layer and the electrode. A bias applied to the detector results in the field configuration shown in Figure 1(b). An incident infrared photon passes through the substrate and interacts in the Si:As layer, generating an electron/hole pair. Under the effect of the electric field, the electron drifts quickly to the blocking layer. The increased field near the blocking layer (BL) (see Figure 1(b)) provides a high cross-section for impact ionization, resulting in an avalanche of electrons with a typical gain of $\sim 10^4$. The electrons are collected at the electrode in timescales of a few nanoseconds, while the holes drift more slowly to the opposite electrode implanted in the silicon substrate. Detector dark current arises primarily from thermal generation in the Si:As layer. For a more detailed description of the SSPM device physics, see Petroff *et al.* (1987).

3. Cryostat

Due to the operating requirements of the SSPM (detector temperature < 10 K) and its long-wavelength response, the SSPM must be cooled with liquid helium. We house the SSPM in an Infrared Laboratories dewar (see Figure 2 for schematic) with a typical hold time of $\sim 8 - 10$ hours. Light enters the dewar through a fused silica entrance window, and then passes through a cold filter (usually a J-, H-, or K-band filter on a thermal blocker which reduces long-wavelength radiation). Immediately after the cold filter comes an aperture stop slide at the focal plane of the telescope, with stop diameters of 0.6 and 0.3 mm (giving 6 arcsec and 3 arcsec fields on the Las Campanas Observatory 2.5-meter telescope). Two fused silica lenses reimage the aperture stop on the detector with a 3:1 ratio. The first lens images the telescope secondary mirror onto a Lyot stop which blocks stray light. The

second lens then brings the light to a focus on the 200x200 micron back-illuminated SSPM, which is mounted on a gold-coated plate along with a temperature-sensing diode and a heating resistor for thermal control.

4. Optical Alignment

In addition to the previously mentioned advantages of speed and photon-counting capability, the unique structure of the SSPM also gives it the ability to be easily aligned with an optical system, which can otherwise be troublesome for back-illuminated single element detectors. The basis of the alignment technique is the interface between the Si:As layer and the undoped Si blocking layer (BL). At room temperature, the As acts as a simple dopant, providing a high concentration of electrons in the conduction band (that is, n-doping). Thus, the interface between the Si:As and the BL forms a photodiode junction at room temperature, sensitive to light out to near the silicon cutoff ($\sim 1.1\mu\text{m}$). In order for some photons to penetrate the Si substrate and yet still interact at the junction, we must use a fairly bright source with a wavelength just below the cutoff, such as a Nd:YAG $1.06\mu\text{m}$ CW laser.

We performed the alignment of our instrument at the MIT Laser Spectroscopy Lab, using a 300 mW CW Nd:YAG laser. The laser beam was sent into the (open, room-temperature) dewar and aligned with the smallest aperture stop using an IR viewer, retro-reflecting the beam to check orthogonality. We connected the SSPM dewar leads to a simple circuit such as is commonly used for reversed-bias operation of photodiodes. We placed a chopper wheel in the laser beam path, and connected the SSPM signal to an SR560 amplifier (see below) with both high- and low-frequency filtering selected to minimize noise while passing the chopper frequency. The signal was easily readable on an oscilloscope,

with typical amplitudes of ~ 100 mV, and noise amplitudes of ~ 10 mV. The position of the SSPM plate was then manually adjusted to provide the maximum signal.

5. Electronics

Figure 3 show the SSPM electronics chain for telescope observations. A variable potentiometer outside the dewar controls the detector bias, and a $3.9M\Omega$ resistor acts as a current-limiter to prevent detector breakdown. The other terminal of the detector is connected to a room-temperature transimpedance amplifier (TIA) ($R= 100M\Omega$) mounted directly outside the dewar. The TIA acts as a current-mode preamplifier, converting the avalanche current to an output voltage. Photon events produce typical amplitudes of ~ 120 mV at the TIA output, while the RMS noise is typically < 15 mV. The TIA is then fed through a Stanford Research SR-560 amplifier with gain ~ 5 , which is typically mounted on the telescope near the instrument. The amplifier output feeds into a Stanford Research SR-400 digital photon counter. We set the SR-400 discriminator level to cleanly separate real photon events from noise. One SR-400 output feeds a PC real-time display, which facilitates target acquisition and data monitoring throughout the observation. The second SR-400 output is a digital logic pulse to a data recording system. We measure the time resolution of the entire detector+electronics system (limited by the post-detector electronics) to be $\sim 0.2\mu s$, with dead-time of $\sim 0.8\mu s$ per count.

The data recording system we use is the "Lil Wizard Pulsarator" built by Richard Lucinio of Caltech and Jerome Kristian of the Carnegie Observatories. The heart of the Wizard is 2 sets of 2 counting registers. One register accumulates counts from the SR-400 output, while the other counts a preset number of oscillations from a Rubidium (Rb) frequency standard (user-selectable register integration times range from $5\mu s$ to 64 ms).

When the Rb register reaches the preset limit, the counting function switches to the other set of registers, and the first data register is transferred to a buffer. After the buffer accumulates 8192 data elements, it is flushed to an Exabyte tape drive, along with header information including the number of Rb oscillations since power-up. Thus, the Wizard provides continuous data recording while maintaining phase coherence to the accuracy of the Rb frequency standard (typical Allan variance $\sim 10^{-12}$ s/s), even over several separate nights of observation.

6. Laboratory Tests

We have evaluated the performance of our SSPM instrument in the laboratory, using a standard infrared test setup. A blackbody cavity with a pinhole aperture illuminates a 45-degree flat mirror through a variable-speed chopper wheel. The blackbody beam is either fed into the SSPM optics directly from the flat mirror (for most measurements), or else is reflected off a scanning flat mirror, and then into the SSPM optics (for measuring the instrument beam profile). We have measured the instrument dark current and JHK quantum efficiency across a wide range of detector temperatures and bias. Typical quantum efficiency and dark current are plotted in Figures 4 and 5. Taking these data, along with estimates or measurements of background for a band, field of view, and telescope, we can derive the relative signal-to-noise for the various combinations of temperature and bias. Figure 6 shows an example curve for H-band observations on the MMT with a 2-arcsec field of view. We use such curves to select the optimal operating parameters for a given observation.

7. Observational Results

We have used the SSPM high-speed photometer on several telescopes, including the Whipple Observatory 1.2-meter, the Las Campanas 2.5-meter, and the Multiple Mirror Telescope. Some of the most striking examples of the SSPM’s capabilities are shown in Figure 7. Figure 7(a) shows a J-band ($1.25\mu\text{m}$) pulse profile of the 33 ms Crab Nebula pulsar with $20\mu\text{s}$ time resolution. Taking advantage of this high time resolution, we have found trends in the pulse shape as a function of wavelength (Ransom et al., 1994; Eikenberry et al., 1996ab), including changes in the peak-to-peak separation and the peak half-widths on timescales $\sim 100\mu\text{s}$, which are providing new challenges for models of the pulsar emission mechanism. Previous infrared photometers have lacked the time resolution to detect these effects (by an order of magnitude).

Figure 7(b) shows the H-band pulse profile of Hercules X-1, an X-ray pulsar. While the time resolution on these 1.2 s pulses is unremarkable, the sensitivity of the observation is exceptional. The Figure 7(b) profile, which results from a 1 hour observation on the Whipple 1.2-meter telescope, has a $\sim 4\sigma$ significance. Observations with previous detectors (e.g. Middleditch, Pennypacker, and Burns, 1984) have required 3 hours on 3-meter telescopes to obtain slightly weaker detections. From these observations, we have determined the 3σ sensitivity of the instrument to a Crab-like pulse profile to be 1.4×10^{-4} Jy (H=17.3) (1.2-meter telescope), 3.6×10^{-5} Jy (H=18.8) (2.5-meter telescope), and 1.2×10^{-5} Jy (H=20.0) (MMT) for a 1 hour observation. The SSPM sensitivity scales according to the following equation

$$\frac{S}{N} = \frac{\eta F_{sig} t_{obs}}{\sqrt{[n_D + \eta(F_{sig} + F_{sky}) \Delta\lambda A \Omega] t_{obs}}}, \quad (1)$$

where S/N is the signal-to-noise ratio, η is the SSPM quantum efficiency, F_{sig} is the signal photon flux density (photons per square centimeter per micron per square arcsecond per second), t_{obs} is the observation time in seconds, n_D is the SSPM dark count rate (counts

per second), F_{sky} is the sky background photon flux density, $\Delta\lambda$ is the bandpass (microns), A is the telescope area (square centimeters), and Ω is the field of view (square arcseconds).

The sensitivities given above also allow a direct comparison between the SSPM and other types of high-speed infrared photometers. As none of these others are actual photon counters, their noise will have a \sqrt{f} dependence, where f is maximum sampling rate - the electronic bandwidth for analog detectors (e.g. single-pixel devices), or the read rate for digital detectors (e.g. array detectors). We plot the relative signal-to-noise for the SSPM versus a single-pixel InSb detector (Lundgren, 1994) in Figure 8. Again, the response curve for all non-photon-counting detectors will have the shape shown by the InSb detector, while the SSPM curve is flat with respect to sample rate. Thus, at speeds greater than ~ 100 Hz, the SSPM becomes the IR detector of choice.

8. Other Applications

In addition to the observations mentioned above, we are using the current SSPM photometer in a wide range of other astronomical applications. In the area of pulsar research, we are searching for infrared pulsations from SN1987A and other supernova remnants. We have also observed other known pulsars (such as the optical pulsar 0540-69) and compact objects to search for infrared pulsations. A brief list of observed targets includes pulsars (PSR0540-69, PSR1257+12, PSR1957+20, Geminga, PSR1509-58), supernova remnants (SN1987A), soft gamma-ray repeaters (SGR1806-20, SGR1900+14), cataclysmic variables (RW Sextans), black hole candidates (J0422+32), and globular clusters (M15). While we have found no pulsar signals in these preliminary searches, we plan to continue these searches in the future.

Besides the research geared toward compact objects, the SSPM may be extremely

useful in the field of IR adaptive optics. In adaptive optics, one of several corrections is the global wavefront, or "tip-tilt" correction. Previously, both global and local wavefront corrections have been done in the visible, even though the science detectors usually operate in the near-IR (e.g. Lloyd-Hart *et al.*, 1995). Since the Earth's atmosphere possesses differential dispersion between the optical and IR wavebands, the actual distortion being corrected may differ significantly between the optical and the IR. Thus, several groups are investigating the construction of adaptive optics systems with IR tip-tilt correction, sampling from 40-100 Hz (M. Lloyd-Hart, personal communication). While the current SSPM is competitive with "standard" detectors only at the high end of this range, work on future SSPM instruments (see next section) will almost certainly alter this state of affairs dramatically.

9. Future Instrument Development

As mentioned above, the current back-illuminated instrument is the fastest and most sensitive astronomical high-speed IR photometer yet built. However, we have considerable room for improvement, especially in the area of quantum efficiency (typically $\sim 1\%$ for J-, H-, and K-bands). The back-illuminated SSPM is limited in QE at these wavelengths by the relatively short path length of the incident photons through the sensitive region (typically $\sim 25 - 45\mu\text{m}$), compared to the typical absorption length ($\sim 1\text{ mm}$). RISC has found one solution in the edge-illuminated SSPM, which is similar to the back-illuminated SSPM, but, as its name suggests, is illuminated from the side, resulting in a path length of order $1000\mu\text{m}$. Using this technique, RISC has achieved near-infrared quantum efficiencies of $\sim 30 - 40\%$ in laboratory tests. We are currently building a 2nd generation instrument employing an edge-illuminated SSPM as the detector.

The principle problem we have encountered in building this instrument is the small area \times solid-angle product of the detector. In order to achieve maximum response, the detector requires an input beam of $f/3$ or slower. However, given the $45\mu\text{m}$ dimension of the sensitive area, this corresponds to a field of view of only ~ 0.75 arcsec on a 4-meter telescope. In order to increase this field, we use an optical system that feeds the detector with an $f/1$ beam, resulting in a more practical 2.3 arcsec field. By calculating the average path length through the detector, we estimate that this will reduce the effective quantum efficiency by $\sim 35\%$, to a final value of $\sim 25\%$.

Given measurements of sky backgrounds with the present instrument and of the dark current from the edge-illuminated detector, we conclude that the edge-illuminated SSPM should produce a factor of ~ 6 improvement in sensitivity over the current SSPM. Thus, we expect that our 3σ detection limit for a 1 hour observation will be 2.5×10^{-5} Jy (H=19.2) for a 1.2-meter telescope, 6.3×10^{-6} Jy (H=20.7) for a 2.5-meter telescope, and 1.9×10^{-6} Jy (H=22.0) for the MMT.

We thank RISC for supplying the SSPMs, and especially K. Hays and M. Stapelbroek for their invaluable advice and help, and R. Florence for his continued support of infrared astronomical instrument development; J. Middleditch, C. Pennypacker and J. Kristian for their support of the SSPM project in both development and observations; J. Geary, S. Willner, C. Hughes, and P. Crawford for their assistance in designing and assembling both instruments at the CfA; D. Paolucci and the MIT Laser Spectroscopy Lab for help with the laser alignment; Bill Riley and EG & G for supplying the Rubidium frequency standard; R. Narayan for providing funding support; and, R. Lucinio for maintaining the Wizards. The SSPM project has been supported in part by a Smithsonian Scholarly Studies Grant. S. Eikenberry is supported by a NASA Graduate Student Researchers Program fellowship through NASA Ames Research Center.

REFERENCES

- Cheng, K.S., Ho, C., & Ruderman, M. 1986a, *ApJ*, 300, 500.
- Cheng, K.S., Ho, C., & Ruderman, M. 1986b, *ApJ*, 300, 522.
- Eikenberry, S.S., Fazio, G.G., Ransom, S.M., Middleditch, J., Kristian, J., Pennypacker, C.R. 1996a, *ApJ Letters*, submitted
- Eikenberry, S.S., Fazio, G.G., Ransom, S.M., Middleditch, J., Kristian, J., Pennypacker, C.R. 1996b, *ApJ*, submitted
- Hodapp, K.W., Hora, J.L., Hall, D.N., Cowie, L.L., Metzger, M. Irwin, E.M., Keller, T.J., Vural, K., Kozłowski, L.J., Kleinhans, W.E., 1995, *SPIE Vol. 2475*, 8.
- Lloyd-Hart, M., Angel, J.R.P., Jacobsen, B., Wittman, D., Dekany, R., McCarthy, D., Kibblewhite, E., Wild, W., Carter, B., Beletic, J., 1995, *ApJ*, 439, 455.
- Lundgren, S.C., 1994, *PhD. Thesis*, Cornell University.
- Middleditch, J., Pennypacker, C.R., Burns, M.S. 1983, *ApJ*, 274, 313.
- Petroff, M.D., Stapelbroek, M.G., and Kleinhans, W.W. 1987, *Appl.Phys.Lett.*, 51, 6.
- Pipher, J.L., Forrest, W.J., Wu, J., 1995, *SPIE Vol. 2475*, 428.
- Ransom, S.M., Fazio, G.G., Eikenberry, S.S., Middleditch, J., Kristian, J.A., Hays, K., Pennypacker, C.R. 1994, *ApJ*, 431, L43.

Fig. 1.— (a) SSPM layer configuration with operational schematic, (b) SSPM electric field configuration

Fig. 2.— SSPM instrument schematic layout

Fig. 3.— SSPM electronics layout

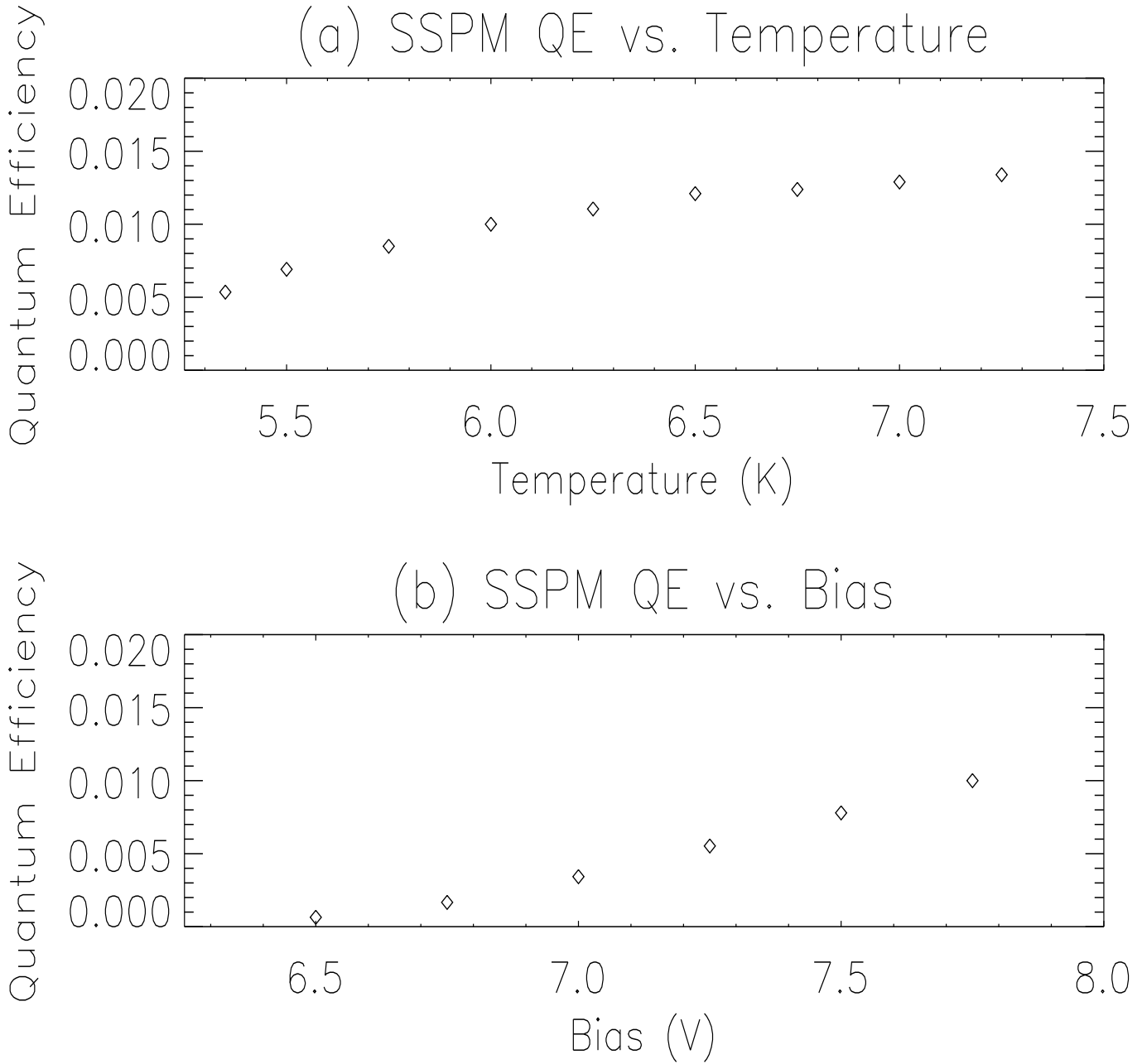


Fig. 4.— (a) SSPM K-band quantum efficiency versus temperature at bias = 7.75 V, (b) SSPM K-band quantum efficiency versus bias at temperature = 6.0 K

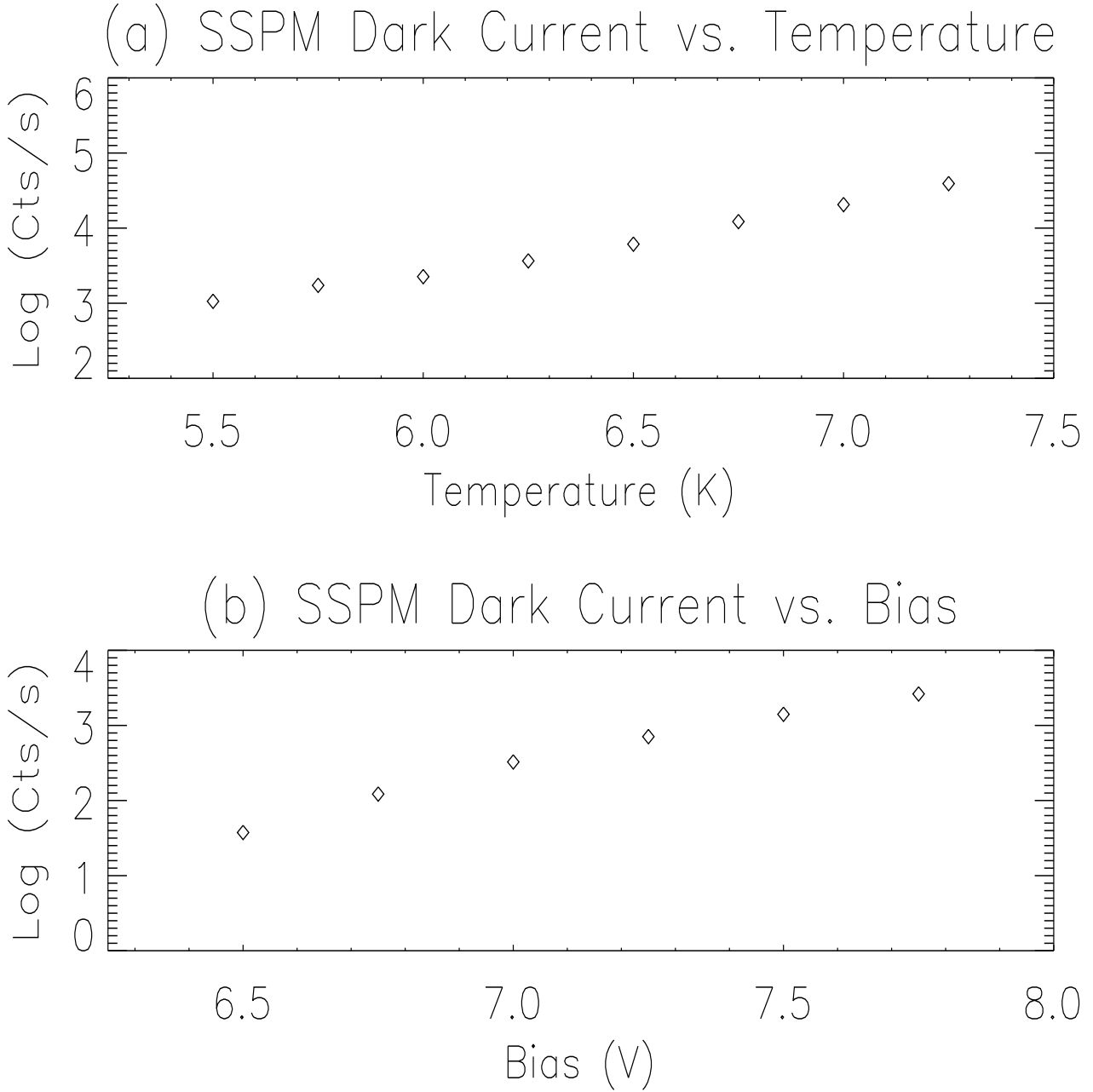


Fig. 5.— (a) SSPM dark current versus temperature at bias = 7.75 V, (b) SSPM dark current versus bias at temperature = 6.0 K

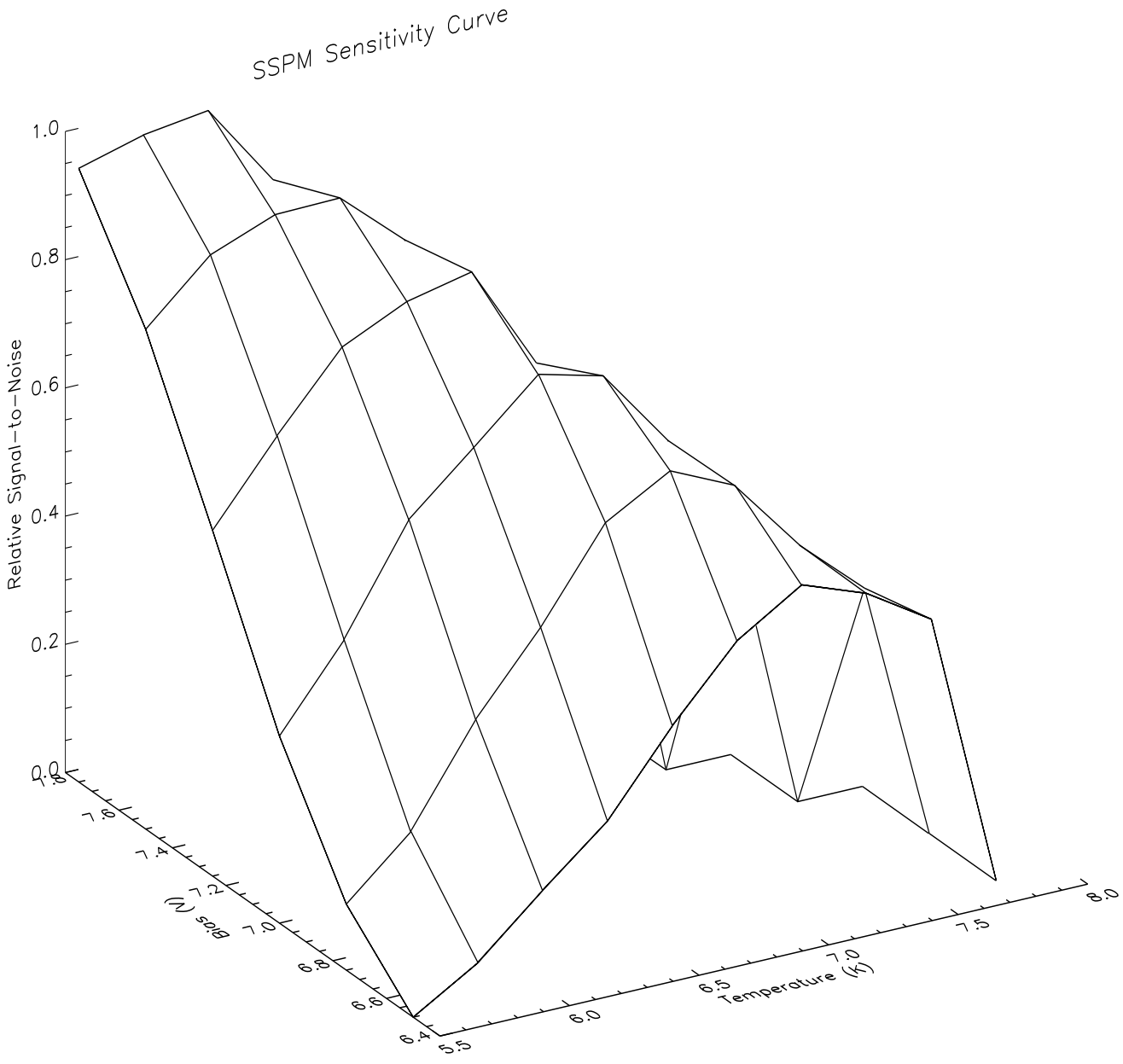


Fig. 6.— SSPM relative signal-to-noise versus temperature and bias

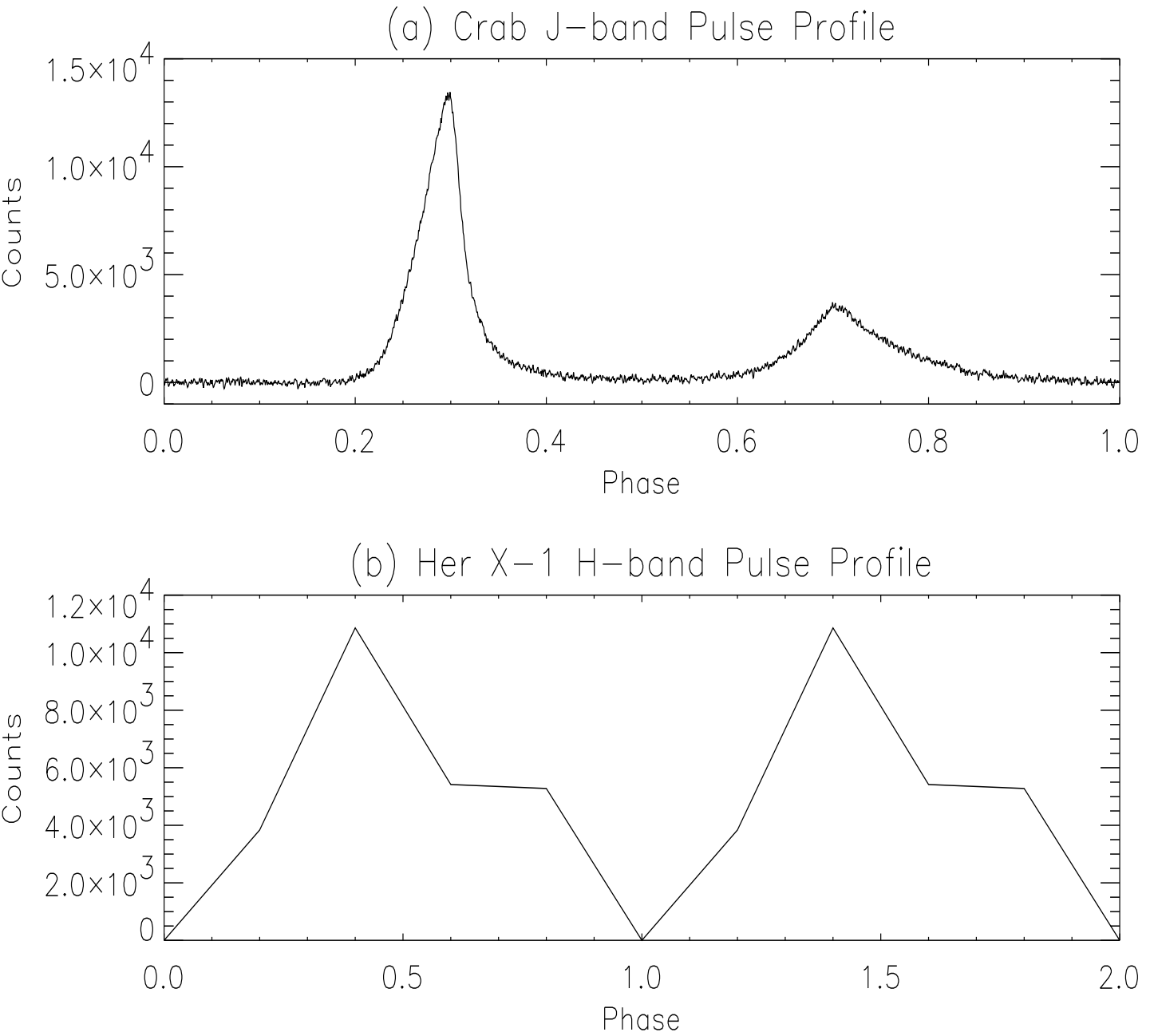


Fig. 7.— (a) Crab Nebula pulsar J-band pulse profile, (b) Her X-1 H-band pulse profile

Detector Sensitivities

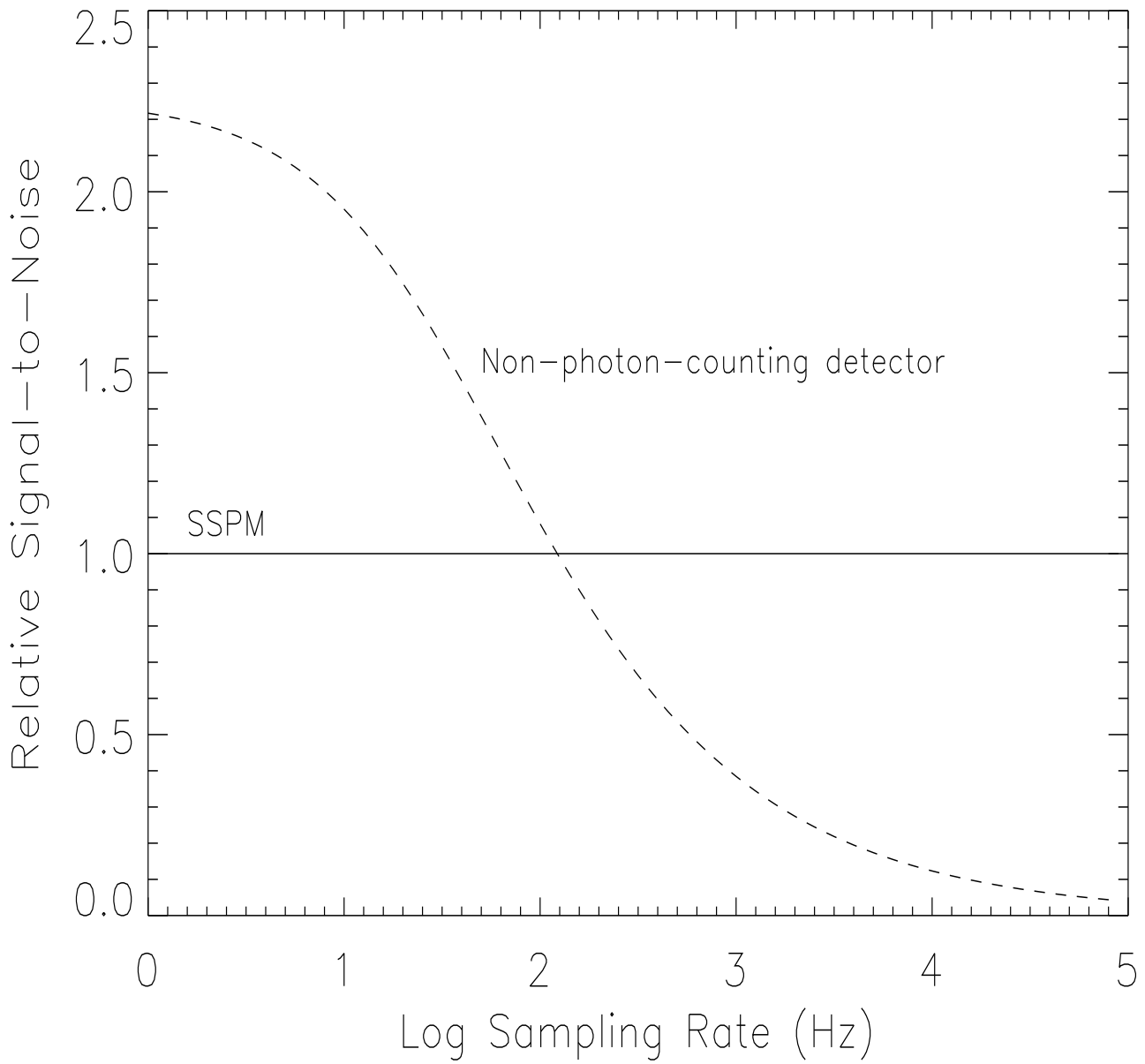


Fig. 8.— Relative signal-to-noise versus sampling rate